A&A 453, 155–162 (2006)
DOI: 10.1051/0004-6361:20054466

Astronomy & Astrophysics

Extended envelopes around Galactic Cepheids

II. Polaris and δ Cephei from near-infrared interferometry with CHARA/FLUOR⋆

A. Mérand[1,3], P. Kervella[1], V. Coudé du Foresto[1], G. Perrin[1], S. T. Ridgway[2,3], J. P. Aufdenberg[2], T. A. ten Brummelaar[3], H. A. McAlister[3], L. Sturmann[3], J. Sturmann[3], N. H. Turner[3], and D. H. Berger[3]

[1] LESIA, UMR 8109, Observatoire de Paris, 5 place Jules Janssen, 92195 Meudon, France
e-mail: antoine.merand@obspm.fr
[2] National Optical Astronomy Observatories 950 North Cherry Avenue, Tucson, AZ 85719, USA
[3] Center for High Angular Resolution Astronomy, Georgia State University, PO Box 3965, Atlanta, Georgia 30302-3965, USA

Received 3 November 2005 / Accepted 11 March 2006

ABSTRACT

We present the results of long-baseline interferometric observations of the classical Cepheids Polaris and δ Cep in the near infrared K' band (1.9−2.3 μm), using the FLUOR instrument of the CHARA Array. Following our previous detection of a circumstellar envelope (CSE) around ℓ Car (Kervella et al. 2006), we report similar detections around Polaris and δ Cep. Owing to the large data set acquired on Polaris, in both the first and second lobes of visibility function, we have detected the presence of a circum-stellar envelope (CSE), located at 2.4 ± 0.1 stellar radii, accounting for $1.5 \pm 0.4\%$ of the stellar flux in the K band. A similar model is applied to the δ Cep data, which shows improved agreement compared to a model without CSE. Finally, we find that the bias in estimating the angular diameter of δ Cep in the framework of the Baade-Wesselink method (Mérand et al. 2005b) is of the order of 1% or less in the K band. A complete study of the influence of the CSE is proposed in this context, showing that at the optimum baseline for angular diameter variation detection, the bias is of the order of the formal precision in the determination of the δ Cep pulsation amplitude (1.6%).

Key words. stars: variables: Cepheids – stars: circumstellar matter – stars: individual: Polaris (α Ursae Minoris) – stars: individual: δ Cephei – techniques: interferometric – techniques: high angular resolution

1. Introduction

Using low resolution interferometry (e.g. small baselines at which the star is under resolved) in the near infrared and mid-infrared, we recently reported the discovery of a circumstellar envelope (CSE) around the 35 day period Cepheid ℓ Car (Kervella et al. 2006). The presence of this feature may disturb the application of the classical Baade-Wesselink (BW) method, which aims at determining distances by measuring simultaneously the variations of angular and linear diameters.

Stellar interferometry has demonstrated a capability to measure precise Cepheid distances and the calibration zero point of the their Period-Luminosity relation (Kervella et al. 2004a). With the recent calibration of the BW method, thanks to the direct p-factor measurement by interferometry (Mérand et al. 2005b), it is now mandatory to study the Cepheid center-to-limb darkening (CLD) and the possible presence of CSEs in order to constrain two of the last sources of possible bias in the interferometric BW method. A morphological model is required in order to derive the angular diameter from a single baseline visibility measurement. If the assumed CLD differs from the actual one, or if the circumstellar emission is present, the derived angular diameters can be biased, possibly leading to a biased distance estimation in the BW method.

Following our recent study of ℓ Car, we present in this work near infrared observations of Polaris (α UMi, HR 424, HD 8890) and complementary observations of δ Cep (HR 8571, HD 213306) using the FLUOR (Fiber Link Unit for Optical Recombination) beam combiner installed at the CHARA (Center for High Angular Resolution Astronomy) Array. Polaris is the brightest Cepheid in the northern skies and offers the best opportunity to measure the CLD and detect the presence of a CSE. A great amount of data was collected, 65 calibrated data points using 4 different baselines (projected length from 19 to 246 m), to disentangle the CLD and CSE characterization from the possible close companion and radial pulsation detection. We show that these two latter effects have not been detected in our dataset, whereas the presence of a CSE is mandatory to explain a visibility deficit observed at $V^2 \sim 50\%$, as in ℓ Car.

We also present complementary observations of the Cepheid δ Cep with medium baselines ($B \approx 150$ m), following our determination of its p-factor using very long baselines (Mérand et al. 2005b). The final characteristics of the CSEs detected around Polaris and δ Cep are qualitatively in agreement with what has been found for ℓ Car.

Finally, we present a formal analysis of the bias introduced to the BW method in presence of the CSE.

2. Observational setup

2.1. CHARA/FLUOR

Observations were undertaken in the near infrared (K' band, $1.9 \leq \lambda \leq 2.3$ μm) at the CHARA Array (ten Brummelaar et al. 2005) using FLUOR, the Fiber Linked Unit for Optical

⋆ Table 4 is only available in electronic form at the CDS via anonymous ftp to cdsarc.u-strasbg.fr (130.79.128.5) or via http://cdsweb.u-strasbg.fr/cgi-bin/qcat?J/A+A/453/155

Recombination (Coudé du Foresto et al. 2003). The FLUOR Data reduction software (DRS) (Coudé du Foresto et al. 1997; Kervella et al. 2004b), was used to extract the squared modulus of the coherence factor between the two independent apertures from the fringe pattern.

2.2. Baselines

The baselines were chosen according to the Polaris and δ Cep angular sizes (approximately 3 and 1.5 mas, respectively), wavelength of observation and desired spatial resolution. Polaris must be observed at i) low spatial resolution ($V^2 \sim 50\%$) in order to detect the CSE and the possible faint companion, ii) high resolution (in the first lobe of the visibility profile, near the first null) in order to detect the pulsation with optimum sensitivity and iii) at the top of the second lobe in order to measure the CLD. This led to the choice of CHARA baselines i) S1-S2 ($b = 33$ m), E1-E2 ($b = 66$ m), ii) W2-E2 ($b = 156$ m) and iii) W1-E2 ($b = 251$ m). Concerning δ Cep, the only requirement for the complementary data was to reach $V^2 \sim 50\%$, where the CSE is believed to be easily detectable. This criteria led to projected baselines of roughly 150 m, corresponding to W2-E2 and S2-W2 at the CHARA Array. These latter baselines were chosen with similar length but different orientation, in order to investigate possible asymmetry in the CSE, if present.

2.3. Calibrators

Calibrator stars were chosen in two different catalogs: B02 (Bordé et al. 2002) for stars larger than 2.0 mas in diameter and M05 (Mérand et al. 2005a) for stars smaller than 2.0 mas using criteria defined in this latter work (see Table 1). We used calibrators from B02 for baselines smaller than 100 m, while for larger baselines we used calibrators from M05. The two catalogs are very similar by their characteristics: M05 is an extension of B02 using the very same procedure to estimate angular diameters. Therefore no trend is expected when using data calibrated with stars coming from these two catalogs.

3. Observations of Polaris

3.1. Context

Polaris has the largest angular size of all northern population I Cepheids. This star is therefore the best candidate for CLD measurements using an interferometer.

Because Polaris lies near the North celestial pole, the projected baseline remains almost constant in length while varying in position angle during the night (see Fig. 1).

3.2. Expected hydrostatic CLD profile

Claret (2000) tabulated limb darkening coefficients from hydrostatic ATLAS models. If we use the following parameters $T_{\rm eff} = 6000$ K, $\log g = 2.5$ and solar metallicity, we get in the database the following LD coefficients for the K band:

$$a_1 = 0.6404, a_2 = -0.1182, a_2 = -0.2786, a_4 = 0.1802$$

describing the center to limb variations:

$$I(\mu)/I(1) = 1 - \sum_{k=1}^{4} a_k \left(1 - \mu^{k/2}\right). \quad (1)$$

Table 1. Calibrators used for the observations. "SP" stands for spectral type. Uniform Disk diameters, given in mas, are only intended for computing the expected squared visibility in the K band.

	SP	UD diam.	Baseline	Notes
HD 5848	K2 II-III	$2.440_{\pm 0.064}$	S1-S2	B02, 1
HD 5848	K2 II-III	$2.440_{\pm 0.064}$	E1-E2	B02, 1
HD 81817	K3 III	$3.260_{\pm 0.085}$	–	–
HD 139669	K5 III	$2.890_{\pm 0.035}$	–	–
HD 222404	K1 III-IV	$3.290_{\pm 0.051}$	–	–
HD 83550	K2 III	$1.160_{\pm 0.015}$	W2-E2	M05, 1
HD 91190	K0 III	$1.330_{\pm 0.018}$	–	–
HD 118904	K2 III	$1.411_{\pm 0.018}$	–	–
HD 176527	K2 III	$1.721_{\pm 0.024}$	–	M05, 2
HD 218452	K5 III	$2.080_{\pm 0.024}$	–	–
HD 162211	K2 III	$1.598_{\pm 0.020}$	S2-W2	M05, 2
HD 165760	G8 III	$1.500_{\pm 0.020}$	–	–
HD 207130	K1 III	$1.331_{\pm 0.017}$	–	–
HD 217673	K1 II	$1.411_{\pm 0.020}$	–	–
HD 9022	K3 III	$1.050_{\pm 0.014}$	W1-E2	M05, 1
HD 42855	K3 III	$0.803_{\pm 0.010}$	–	–
HD 217673	K1 II	$1.411_{\pm 0.020}$	–	–
HD 206842	K1 III	$1.214_{\pm 0.016}$	–	M05, 2

Notes: B02 refers to Bordé et al. (2002) catalog; M05 to Mérand et al. (2005a) catalog; 1 refers to Polaris observations and 2 refers to δ Cep ones.

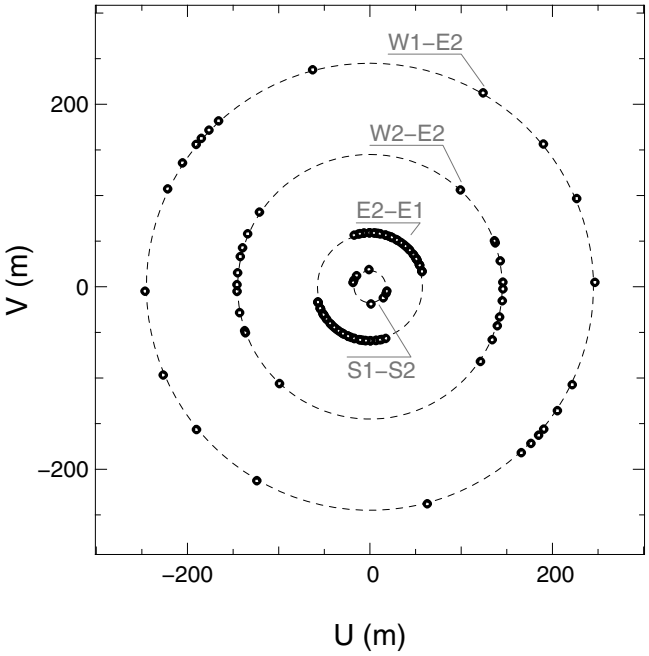

Fig. 1. $u-v$ map, in meters. Up is north and right is east. Each data point lies on a circle corresponding to the baseline because of the near-polar position in the sky of Polaris.

It is necessary to take into account the bandwidth smearing. Once the monochromatic visibility $v(\sigma, b)$ is computed from the intensity profile $I(\mu)/I(1)$ for a given wavenumber $\sigma = 1/\lambda$ and baseline b, the wide-band squared visibility is obtained by computing:

$$\mathcal{V}^2_{\rm FLUOR}(b) = \frac{\int T_r^2(\sigma)\ (B(\sigma)/\sigma)^2\ v^2(\sigma, b)\ {\rm d}\sigma}{\int T_r^2(\sigma)\ (B(\sigma)/\sigma)^2\ {\rm d}\sigma} \quad (2)$$

where $B(\sigma)/\sigma$ is the black body Planck function, in number of photons per unit of time, frequency and surface area for the effective temperature of the star (since FLUOR uses a detector that

Table 2. Best fit model parameters for Polaris and its CSE. $\theta_\star$ is the stellar angular diameter (mas), α the CLD coefficient, θ_s the shell angular diameter (mas), w the shell width (mas) and $F_s/F_\star$ the relative brightness (Fig. 3). Last column tabulates the reduced χ^2. Only parameters with error bars (lower scripts) have been fitted. The first line is the hydrostatic model; the second line is the adjusted CLD; the model of the last line includes a shell.

$\theta_\star$	α	θ_s	w	$F_s/F_\star$	χ^2
$3.152_{\pm 0.003}$	0.16	–	–	–	4.5
$3.189_{\pm 0.005}$	$0.26_{\pm 0.01}$	–	–	–	2.5
$3.123_{\pm 0.008}$	0.16	$7.5_{\pm 0.2}$	0.5	$1.5_{\pm 0.4}\%$	1.4

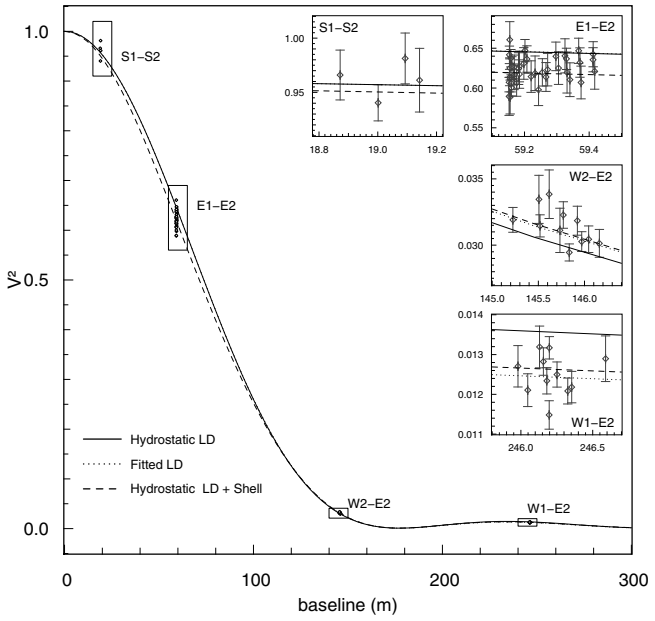

Fig. 2. Results of fit for different models. Squared visibility with respect to baseline. Solid line is the hydrostatic CLD from Claret (2000), dotted line is a fitted power law CLD while the dashed line is the hydrostatic model surrounded by the shell (see Table 2 for the models parameters). Note that solid and dotted line overlap in the main panel, the S1-S2 and E1-E2 small panels.

measures the flux as a number of photons); T_r is the chromatic instrumental transmission, which has been measured internally (a standard atmospheric transmission model is also applied).

The only parameter adjusted in the fit is the angular diameter of the star, which is found to be $\theta_\star = 3.152 \pm 0.003$ mas. The corresponding reduced χ^2 is 4.5 (Table 2). Note that we take into account the correlations between error bars of different data points. These correlations come from the multiple use of a single calibrator in the dataset. They are properly treated according to the formalism developed by Perrin (2003).

In Fig. 2, we display the data points and the models. The solid line corresponds to the hydrostatic CLD model for Polaris from Claret (2000). It appears that the model fails to reproduce the data in the second lobe (see W1-E1 baseline) and marginally intermediate baselines (E1-E2), where $V^2 \sim 50\%$.

3.3. Adjusted center-to-limb variation

Because the second lobe is not well reproduced by the hydrostatic model, a simple way to improve the model is to adjust the strength of the CLD. Indeed, the CLD profile changes the scale of the first lobe (not its shape) and the height of the second lobe. For this purpose we chose a single parameter CLD law, the power law: $I(\mu)/I(1) = \mu^\alpha$ (Michelson & Pease 1921; Hestroffer 1997). The hydrostatic model computed from Claret coefficients for Polaris corresponds to $\alpha = 0.16$. Even using a single parameter CLD model compared to the 4-parameters Claret's law, corresponding V^2 only differ at most by 10^{-3} (relative) in the first two lobes. We therefore prefer to use a single parameter CLD law (the power law), for the sake of simplicity.

The best fit, adjusting α as a free parameter, leads to $\theta_\star = 3.189 \pm 0.005$ mas and $\alpha = 0.26 \pm 0.01$; the reduced χ^2 is then 2.5 (Table 2, second line). Based on the χ^2, the fit is significantly better: the hydrostatic CLD led to χ^2 of 4.5. The CLD is stronger than predicted by hydrostatic models and the corresponding angular diameter is thus larger, as expected. However, before trying to interpret this result in terms of photospheric characteristics, one should notice that this model still fails to fit the mid-first lobe (see E1-E2 panel in Fig. 2, dotted line, which actually overlaps with the solid line). The measured V^2 data are lower than computed for a limb darkened disk. A change in CLD affects primarily the second lobe (higher spatial frequencies), and only the scale of the first lobe. In order to change the shape of the first lobe, one has to invoke something larger that Polaris itself to disturb the lower spatial frequencies. Thus, we think that this strong CLD is not realistic.

3.4. Companion and pulsation

When seeking possible explanations for the departure around $V^2 \sim 50\%$, two obvious possibilities must be considered before invoking a CSE: Polaris is a pulsating star and a spectroscopic-astrometric binary as well (Wielen et al. 2000). We shall now show that neither of these two hypotheses can explain the discrepancy in the first lobe.

If the departure detected at V^2 is believed to be due to the companion, it should vary with the position angle angle of the projected baseline. Our sampled range in projection angle is quite large and densely populated for E1-E2 (Fig. 1). However the departure does not change significantly with respect to projection angle of the baselines. As seen in Fig. 2: the V^2 recorded using E1-E2 are consistent within their errors. Because our typical V^2 precision is of the order of 3%, the companion must be as faint as 1.5% of the main star flux, or less (in the K band), in order to remain undetected by CHARA/FLUOR. Moreover, based on non detection in UV and X-ray, Evans et al. (2002) estimate that the companion mass is between 1.7 and 1.4 solar masses. Thus, this star is most likely a main sequence star of similar spectral type (but lower luminosity) to Polaris. Wielen et al. (2000), in their study of the astrometric orbit, conclude that the difference in magnitude between the two components is $\Delta V = 6.5$ from which we deduce, because of the similarity in spectral type, $\Delta K \approx 6.5$. This corresponds to a flux ratio of 2.5×10^{-3} which translates into an interferometric V^2 modulation twice as large, 5×10^{-3} or half a percent.

According to the latest radial velocity surveys, the radial pulsation of Polaris is of the order of 0.4% in diameter (Moskalik & Gorynya 2005). In the case of FLUOR, for which the relative error in squared visibility (σ_{V^2}/V^2) is almost constant, the most effective baseline to search for diameter variations maximizes the following criterion: for a given baseline b and angular diameter θ, a diameter increase of $\delta\theta$ should lead to the maximum relative increase in squared visibility $\delta V^2/V^2$. Thus, the

optimum baseline maximizes (in absolute value) the dimensionless quantity A_f, which we call the amplification factor:

$$A_\mathrm{f} = \frac{\partial V^2(b,\theta)}{\partial \theta} \frac{\theta}{V^2(b,\theta)}. \quad (3)$$

If the angular diameter θ increases by the very small amount $\delta\theta$, then, the visibility increases by $\delta V^2/V^2 = A_\mathrm{f} \times \delta\theta/\theta$. If we compute A_f for the four projected baselines for which Polaris has been observed, we get -0.1, -1, -11.5 and -3.7 for S1-S2, E1-E2, W2-E2 and W1-E2 respectively. Note that A_f is negative in the first lobe: an increase in diameter leads to a decrease in visibility, a well known effect of the Fourier transform. Our best baseline to detect the pulsation on Polaris is W2-E2 with an amplification factor of -11.5. Our relative average calibrated V^2 uncertainty is of the order of 3.5% for this baseline, thus we should be able to detect a 0.3% pulsation amplitude within one sigma (respectively 1% within 3 sigmas), assuming good phase coverage. In our case, data were recorded on three nights within a week. Because the pulsation is almost a multiple of 1 day ($P \approx 3.97$ days), it was not possible to explore more than three different epochs, one quarter phase apart. Fitting a uniform non-pulsating disk to W2-E2 data leads to a reduced χ^2 of 1.05, which means the pulsation was not detected due to poor phase coverage or because its amplitude was slightly shallower than expected (0.5%).

3.5. CSE model

We demonstrated that neither the companion nor the pulsation can be detected in our dataset. These phenomena cannot explain the visibility departure we observed at $V^2 \sim 50\%$ and can be therfore neglected.

Following the study on ℓ Car, we shall now explore the possible presence of a CSE around Polaris. We will adopt a ring-like model for the CSE. The image of the object, as seen by the interferometer, is supposed to be a limb-darkened star, surrounded by a ring. Note that the ring does not represent a flat disk, it is the two dimensional projection of the surrounding shell. This model contains five parameters (see Fig. 3): the star angular diameter ($\theta_\star$), its limb darkening coefficient (α), the ring mean diameter (θ_s), its width (w) and the flux ratio between the two components $F_\mathrm{s}/F_\star$. Apart from a star surrounded by a ring, this model can reproduce a single star ($F_\mathrm{s}/F_\star = 0$) or a star with an uniformly bright environment ($\theta_\mathrm{s} - w = \theta_\star$).

3.6. Results

The number of parameters (5) is too large compared to our dataset. Not that we do not have enough data points, but because these data points are bundled in four sets, one for each baseline. This is due to the particular position of Polaris in the sky (near the pole) and because our model is centro-symmetric. We choose to fix the center to limb darkening coefficient to the value predicted by hydrostatic models ($\alpha = 0.16$). Moreover, we also realized that the ring width does not play a significant role in the minimization: we fixed this parameter to different values, from 0.01 mas (very sharp ring) to 1 mas (diluted ring) and always obtained results for the other parameters within one sigma error bar. This is probably due to our lack of spatial resolution, which prevented us to actually resolve the ring width. Finally, only three parameters were adjusted: the stellar angular diameter, the shell angular diameter and its flux ratio. The best model is a CSE accounting for $1.5 \pm 0.4\%$ of the stellar flux and 7.6 ± 0.2 mas in angular diameter, whereas the stellar angular diameter is 3.123 ± 0.008 mas. The reduced χ^2 is 1.4 (Table 2).

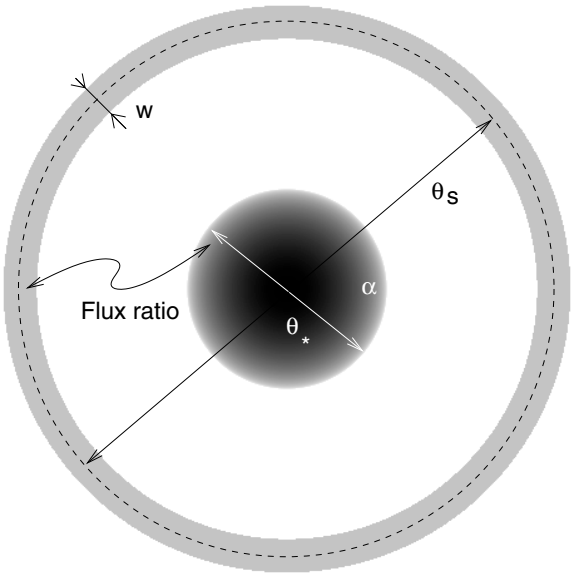

Fig. 3. Our simple CSE model: a star and a ring, as seen by the interferometer. The star (in the center) is characterized by its angular diameter $\theta_\star$ and CLD coefficient α (darker means brighter), whereas the shell is characterized by its angular diameter θ_s, width w and flux ratio.

Interestingly, though the CLD has the same as before ($\alpha = 0.16$, solid line in the same figure), the second lobe is lower than in the model without an envelope: the shell lowers the second lobe. This can be explained easily: since the shell is completely resolved at these baselines (its own visibility is extremely low), it only contributes as an uncorrelated flux and reduces the visibility by a factor $F_\star/(F_\mathrm{s} + F_\star)$ where $F_\star$ and F_s are the total fluxes of the two components (star and shell respectively).

3.7. Influence of the CLD

The CLD cannot be constrained from our data, not because they are not sensitive to it (we do have data in the second lobe), but rather owing to the limited number of free parameters the $u - v$ coverage authorizes. In terms of least square minimization, the reduced χ^2 is already close to its reasonable minimum. Adding a free parameter does not improve the fit – worse, it complicates the minimization algorithm and the error bar estimations. The only thing allowed, is to explore changes in the fixed value for the CLD parameter.

The χ^2 does not change much but it is still interesting to watch the behavior of the free parameters. The main effect of changing the CLD is to change the stellar diameter accordingly. Indeed, this is just a well known effect of the limb darkening, as the equivalent uniform disk diameter remains the same. The second lobe changes slightly, as expected: increasing the strength of the CLD lowers the second lobe. More interestingly, the flux ratio between the CSE and the star changes significantly. We previously noted that the shell would lower the second lobe. If the CLD lowers it too, the shell does not have to be as bright to compensate the effects of a shallow CLD. Yet it is not possible to let the shell disappear completely: the V^2 deficit still has to be fitted. Furthermore, the size of the shell does not change, since it is not constrained by the second lobe but by the position (in term of baseline) of the deficit at low spatial frequencies.

Therefore it is not possible to draw conclusions regarding Polaris' intrinsic CLD. We chose not to constrain this parameter and fixed it to a plausible value. Firstly, the quality of the fit is good enough (as judged by χ^2) to conclude that this value is compatible with our data set. Secondly, our model is not realistic enough that we can hope measuring the CLD with good accuracy. However, we suggest that the CLD of Polaris is probably consistent with the value expected from hydrostatic simulations.

3.8. Nature of the ring

We tested our best fit geometry with a physical model, such as the one used by Perrin et al. (2004) for Mira stars: this model is a simple radiative transfer calculation for a single layer shell surrounding a star. The shell is a self emitting black body, like the star itself. This type of model and our ring model lead to similar geometries for the object, as seen by the interferometer. In the model described by Perrin et al. (2004), the shell temperature can be computed using a simple radiative equilibrium model, such as presented in Ireland et al. (2005). Using silicate opacities (Suh 1999) and a black body spectrum for the Cepheid ($T_{\rm eff} \approx 6000$ K), we found an equilibrium temperature of the order of 2500 K at 3 stellar radii, which does not allow silicate dust grains to survive. Based on this test, the observed circumstellar emission is unlikely to be due to thermal emission from a silicate dust shell. This conclusion does not apply to Mira stars ($T_{\rm eff} \approx 2800$ K), for which the equilibrium temperature is much lower for a shell at the same distance.

3.9. Conclusion

A model consisting in a limb darkened star surrounded by a shell is an important improvement compared over the simple darkened disk model. The first lobe visibility deficit, for E1-E2 baseline, is understood to be due to the presence of a CSE consisting of a dim ring 2.4 ± 0.1 times larger than the star itself. The width of the ring is not known, and can be either thin or extended. However, the flux ratio between the CSE and the star is accurately known and does not depends on the width of the adopted ring: $1.5 \pm 0.4\%$. It is not possible to well constrain the intrinsic CLD of the star. However, our choice of a CLD computed from hydrostatic model (Claret 2000), combined with a CSE lead to a model consistent with the interferometric data.

4. Observations of δ Cep

4.1. Additional observations

In a recent study, we observed δ Cep (Mérand et al. 2005b) and applied the Baade-Wesselink (BW) method to the interferometric V^2 measurements. These measurements were obtained at very long baselines, between 235 and 315 m where $0.02 \leq V^2 \leq 0.15$. This range was chosen from among the whole dataset because it maximized the amplification factor criterion. The remaining data, acquired at medium baselines, did not contribute significantly to the angular diameter determination; moreover, their phase coverage was poor.

It was not possible to even suspect the presence of a shell based only on the longest baseline observations. Considering the experience with Polaris (above) and previously with ℓ Car, it appears the the CSE is only detectable using a combination of several different spatial frequencies. Thus, we here combine the sparse medium baseline data acquired on δ Cep in 2004 with more recent observations, obtained in 2005, at baselines where the CSE should show up clearly, if it exists: $V^2 \approx 50\%$. We shall also use the data set presented in Mérand et al. (2005b) in order to have consistent spatial frequency coverage between $V^2 \approx 50\%$ and the first visibility minimum. The purpose of these observations was to detect the presence of a CSE and study the impact on the angular diameter estimation.

Table 3. Best fit model parameters for δ Cep and its CSE. $\theta_\star$ is the stellar angular diameter (mas), α the CLD coefficient, $\theta_{\rm s}$ the shell angular diameter (mas), w the shell width (mas) and $F_{\rm s}/F_\star$ the relative brightness (Fig. 3). Last column tabulates the reduced χ^2. Only parameters with error bars (lower scripts) have been fitted. Note that in the second line, $\theta_{\rm s}/\theta_\star$, α, w and $F_{\rm s}/F_\star$, are set to the values found for Polaris (see Table 2).

$\theta_\star$	α	$\theta_{\rm s}$	w	$F_{\rm s}/F_\star$	χ^2
$1.480_{\pm 0.002}$	0.16	–	–	–	1.9
$1.476_{\pm 0.003}$	0.16	3.54	0.5	1.5%	1.1

4.2. Disentangling the CSE from the pulsation

In order to disentangle the presence of the CSE from the visibility time-modulation caused by the angular radial pulsation $\theta(\phi)$, we define the pseudo baseline B_{θ_0} as:

$$B_{\theta_0} = B\frac{\theta_0}{\theta(\phi)} \tag{4}$$

where $\theta(\phi)$, the angular diameter variation, is known from our previous BW study, which combined very long baseline observations with high precision radial velocity measurements. If the squared visibility data are plotted with respect to B_{θ_0}, they will match the profile of a star with an angular diameter of θ_0. The choice of θ_0 is arbitrary, and does not change the conclusions of the following discussion: we will use $\theta_0 = 1.475$ mas, the average angular diameter we reported in our precedent work (Mérand et al. 2005b).

4.3. CSE Model

It should be possible, in principle, to fit to δ Cep data a CSE model similar to the one we used for Polaris. However, we realize that the lack of data at the shortest baselines, where $V^2 \approx 90\%$, leads to large uncertainty on the CSE size. Indeed, the estimation of this size relies on the determination of the shape of the V^2 departure from the single star model. Even if the departure is obvious at $V^2 \approx 50\%$ compared to longer baselines, one needs data at short baselines, where V^2 approaches unity. While data collected at medium baselines compared to long baselines determine the lower limit for the CSE size, the comparison between short baselines and medium baselines leads to an upper limit.

Owing of the incompleteness of the δ Cep data set, compared to Polaris, we must use a simpler model, especially concerning the size of the CSE. As a first approximation, we choose to adopt the Polaris model, scaled to the appropriate angular diameter. Compared to parameter values given in Table 2, only $\theta_\star$ is adjusted, while $\theta_{\rm s}/\theta_\star$ is fixed to the value found for Polaris. In parallel, we will fit the angular diameter using a the CLD model adopted in Mérand et al. (2005b). The important result will lie in the difference between the two stellar angular diameter estimates.

The results of the fit (Table 3), as well as the visibility data points with respect to the pseudo baseline, are presented

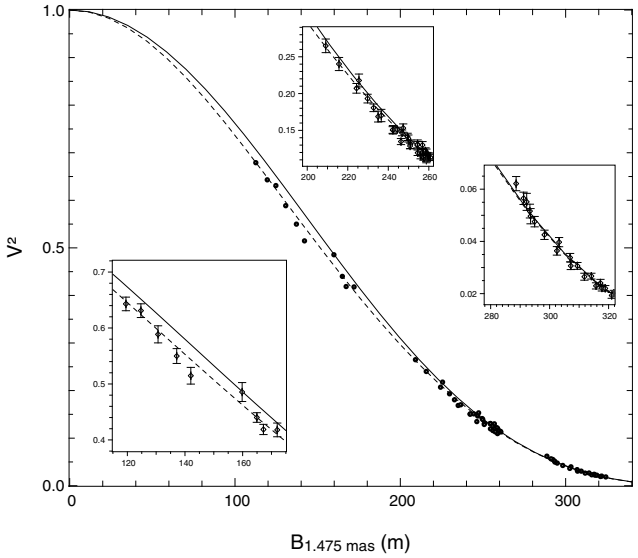

Fig. 4. All δ Cep squared visibility data with respect to the pseudo baseline $B_{\theta_0=1.475\,\mathrm{mas}}$. The limb darkened disk fit appears as a continuous line, while the rescaled Polaris model appears as a dashed line. Both models are fitted to the whole data set, while the rescaling function (pseudo baseline) only affects the longest baselines ($B_{1.475\,\mathrm{mas}} > 200$ m).

in Fig. 4. The revised diameter, using the CSE model, is $\theta_{\mathrm{CLD+CSE}} = 1.476 \pm 0.003$ mas ($\chi^2 = 1.1$) to be compared to $\theta_{\mathrm{CLD}} = 1.480 \pm 0.002$ mas ($\chi^2 = 1.93$) with no CSE. The quantity of interest is the diameter bias β:

$$\beta = \frac{\theta_{\mathrm{CLD}} - \theta_{\mathrm{CLD+CSE}}}{\theta_{\mathrm{CLD+CSE}}}. \quad (5)$$

For our case, considering the whole data set, we found β statistically compatible with 0. This means that omitting the CSE in the morphological model used to derive the angular diameter from our complete δ Cep dataset does not lead to a bias.

It is interesting to note that the Polaris model fits exactly the δ Cep data without any modifications, except for the angular scale.

4.4. CSE symmetry and variability

Two different aspects of the δ Cep CSE can now to be studied: its possible asymmetry and possible relative brightness change during the pulsation phase. The first aspect requires a study at different baseline projection angles of the visibility deficit at $V^2 \approx 50\%$, whereas the second requires a good phase coverage. Our data set contains data at $V^2 \approx 50\%$ with a baseline projection angle range of ninety degrees and with excellent phase coverage (considering our data were acquired at five different epochs).

In order to estimate the possible asymmetry or variability, we should consider the deficit between the measured visibility and that expected from the limb darkened model: $V^2 - V^2_{\mathrm{CLD}}$ at $B_{1.5\,\mathrm{mas}} \sim 140$ m (lower left sub-plot in Fig. 4). This deficit is plotted with respect to the baseline projection angle and pulsation phase in Fig. 5. At our level of precision, the CSE seems to be symmetric and stable through the pulsation. A more elaborate model is thus not justified.

A similar examination of the Polaris measurements leads to the same conclusion – the Polaris CSE appears symmetric and constant in time.

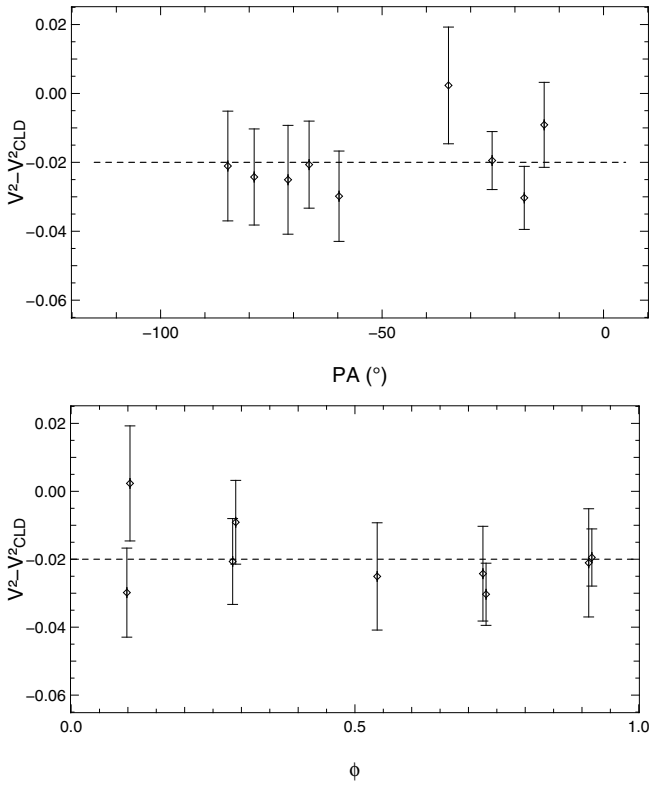

Fig. 5. δ Cep visibility deficit $V^2 - V^2_{\mathrm{CLD}}$ with respect to baseline projection angle (*upper panel*) and pulsation phase (*lower panel*). The dashed line represents a constant deficit. Neither an asymmetry nor a variability of the CSE is detected.

5. Consequences for the Baade-Wesselink method

5.1. De-biasing the stellar diameter measurement

Interferometric angular diameter measurements are always model dependent. In the case of stars without shells, it is necessary to correct for the CLD. In the case of single baseline observations of Cepheids, if a shell has to be taken into account the correction is no longer straightforward and depends on what baseline is used.

To understand this, we should evaluate the multiplicative bias introduced when measuring an angular diameter using a single baseline and not allowing for the presence of the CSE. This approach differs from the previous section, where we considered the whole δ Cep data set. Most Cepheid studies have not benefited from a similarly extensive coverage of spatial frequencies: e.g. Kervella et al. (2004a) or Mérand et al. (2005b). In these latter cases, in order to optimize the use of observing time, interferometric observations were recorded over a very restricted range of baselines.

Let us call $V^2_{\mathrm{CLD}}(b)$ the squared visibility of the star without the shell when observed at the baseline b, and $V^2_{\mathrm{CLD+CSE}}(b)$ for the star with the CSE, at the same baseline. Then, the bias $\beta(b)$ in diameter is, at the first approximation:

$$\beta(b) = \frac{\theta_{\mathrm{CLD}} - \theta_{\mathrm{CLD+CSE}}}{\theta_{\mathrm{CLD+CSE}}} \quad (6)$$

$$= \frac{V^2_{\mathrm{CLD}}(b) - V^2_{\mathrm{CLD+CSE}}(b)}{V^2_{\mathrm{CLD+CSE}}(b)} \times \frac{1}{A_{\mathrm{f}}(b)} \quad (7)$$

where $A_{\mathrm{f}}(b)$ is the amplification factor as defined previously. Note that β is negative: $V^2_{\mathrm{CLD}} > V^2_{\mathrm{CLD+CSE}}$ and $A_{\mathrm{f}} < 0$. In order

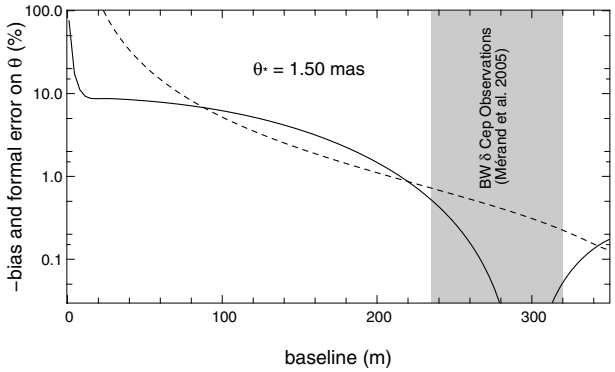

Fig. 6. Bias introduced when determining a Cepheid angular diameter using a single V^2 measurement at a given baseline and not taking into account the presence of the CSE, as a function of projected baseline (solid line). The dashed line is the formal error when deriving the angular diameter from a single V^2 measurement, assuming a 3% error on that measurement. The angular size chosen for this example is the average angular size of δ Cep and its CSE parameters (Table 3). The δ Cep diameter measurements, which took place between 235 and 313 m baselines (gray band), are biased at most at the 1% level, slightly lower than the formal error.

to compare this bias with respect to the formal error in the diameter estimation, we should compute the precision on the angular diameter σ_θ/θ, for a given error in squared visibility σ_{V^2}/V^2:

$$\sigma_\theta/\theta = \left| \frac{\sigma_{V^2}/V^2}{A_\mathrm{f}(b)} \right|. \quad (8)$$

Here, the $V^2_{\mathrm{CLD+CSE}}$ and V^2_{CLD} are essentially equivalent. For numerical application, we will consider the typical result we obtained for Mérand et al. (2005a): $\sigma_{V^2}/V^2 = 0.03$.

Figure 6 shows $-\beta$ for the δ Cep CSE parameters reported in Table 3. Our Baade-Wesselink observations used angular diameters determined at baselines ranging from 235 to 313 m (Mérand et al. 2005b). At such baselines, it appears that the bias is at most of the order of -1%, whereas the diameter formal error is slightly larger. One should notice this is not the case at the shortest baselines, where the bias exceeds the formal error.

5.2. Distance estimation bias

It is important to take into account this bias when applying the BW pulsation parallax method. Indeed, any multiplicative bias in angular diameter will lead to a multiplicative bias in distance, by the same amount. The pulsation parallax equation is (Mérand et al. 2005b):

$$\theta(\phi) - \theta_0 = -2\,\frac{p}{d}\int_0^\phi V_{\mathrm{rad.}}(t)\,\mathrm{d}t \quad (9)$$

where d is the distance, p the projection factor, θ the angular diameter, $V_{\mathrm{rad.}}$ the radial velocity, in the spectroscopic sense – note that we assume that the systematic velocity has been subtracted. The fitted parameters in this equation are θ_0 and d when determining the distance and assuming a given value for p (Kervella et al. 2004a) or θ_0 and p when knowing the distance and determining p (Mérand et al. 2005b). In the case of a multiplicative bias $1+\beta$ on the diameter, the projection factor is biased by the same amount, whereas the distance is biased by $1/(1+\beta)$.

In the case of δ Cep, the angular diameter was at most overestimated by a factor 1.01. Since the star appears larger than it actually is, our formal distance would have been under-estimated. In the case of our previous study, d has been fixed to the estimation of Benedict et al. (2002), $d = 274 \pm 11$ pc. We evaluated p, the projection factor, instead (Eq. (9)). Our value $p = 1.27 \pm 0.06$, should at most be revised to the lower value of 1.26 ± 0.06.

In future high precision interferometric BW observations, it will be necessary to determine and allow for the CSE bias. The best choice, in terms of spatial resolution, will be to observe in the first visibility lobe near the first minimum, in order to maximize the amplification factor. These observations will lead to the best formal angular diameter precision and the lowest bias due to the shell.

This conclusion relies on what we think the CSE looks like in the near-infrared K band. However, it seems likely that the CSE effects on the interferometric angular diameter estimation are less important at shorter wavelengths.

6. Conclusion and discussion

After ℓ Car, we report the interferometric detection in the near infrared of circumstellar emission around two additional Cepheids: Polaris and δ Cep. Polaris was studied in detail and we were able to apply a simple CSE model consisting in a star limb darkened according to hydrostatic models, surrounded by a dim (1.5 ± 0.4% of the stellar flux), 2.4 ± 0.1 stellar diameters CSE. This model also explains the deficit in the visibility profile detected for δ Cep. The three Cepheids have quite different characteristics: Polaris has a small amplitude and a short period; δ Cep has a large amplitude, short period whereas ℓ Car has a large amplitude and long period. The (limited) measurements are consistent with similar circumstellar emission geometries in the three cases studied.

We computed the bias due to the presence of the CSE in the Baade-Wesselink method framework. The bias, in terms of distance, is smallest when the largest first-lobe baselines are used ($V^2 \approx 3$%), and is at most 1%, under the current error contribution of interferometric measurements (Mérand et al. 2005b).

The presence of CSEs, with similar characteristics, around all Cepheids for which sufficient interferometric data are available, raises the possibility that this is a widespread phenomenon. Possible mass loss from Cepheids has been reviewed by Szabados (2003): slight infrared excesses have been detected for almost all Cepheids observed by IRAS, independently of the pulsating period. These observational constraints lead to a mass loss rate of the order of 10^{-10} to 10^{-8} $M_\odot$ yr^{-1}.

Mass loss is expected for Cepheids. This is a consequence of the theoretical Cepheid mass deficit. The deficit is the ratio between two different mass estimates: the evolutionary mass and the pulsational mass. The first, M_e, is derived from the Mass-Luminosity ($M-L$) relation computed from evolutionary numerical codes; the second, M_p, is derived using the Period-Mass-Radius relation (P-M-R), computed from non-linear pulsation numerical codes. The ratio $M_\mathrm{p}/M_\mathrm{e}$ is known to be smaller than unity. Even if the problem has been known for a long time and partially solved by refinements in numerical codes (Cox 1980), recent numerical investigations led to $M_\mathrm{p}/M_\mathrm{e} \approx 0.9$ for galactic Cepheids (Bono et al. 2001). According to these authors, this discrepancy between M_e and M_p might be explained by the fact that evolutionary codes do not take into account mass loss in the He-burning phase (post main sequence). The phase lasts 25 My For a 5 $M_\odot$ Cepheid and 2.5 My for a 11 $M_\odot$, assuming a 10% mass loss, a rough calculation leads to mass loss rates of the order of what is deduced from IRAS measurements.

The direct detection of CSEs around Cepheids at distances of only a few stellar radii is a confirmation that these stars are

experiencing substantial mass loss. The three Cepheids are significantly different one from another: we have three different periods (~4, ~5.4 and ~35 days), thus different masses; different pulsation amplitude (<1% for Polaris and ~15% for ℓ Car and δ Cep). This phenomenon cannot be neglected in future Cepheid studies, presumably having implications for evolutionary and pulsational codes, or while determining distances using the BW method.

Acknowledgements. The authors would like to thank all the CHARA Array and Mount Wilson Observatory day-time and night-time staff for their support during the installation of the FLUOR beam combiner and during the observations presented in this work. The CHARA Array was constructed with funding from Georgia State University, the National Science Foundation, the W. M. Keck Foundation, and the David and Lucile Packard Foundation. The CHARA Array is operated by Georgia State University with support from the College of Arts and Sciences, from the Research Program Enhancement Fund administered by the Vice President for Research, and from the National Science Foundation under NSF Grant AST 0307562.

References

Benedict, G. F., McArthur, B. E., Fredrick, L. W., et al. 2002, AJ, 124, 1695
Bono, G., Gieren, W. P., Marconi, M., Fouqué, P., & Caputo, F. 2001, ApJ, 563, 319
Bordé, P., Coudé du Foresto, V., Chagnon, G., & Perrin, G. 2002, A&A, 393, 183
Claret, A. 2000, A&A, 363, 1081
Coudé du Foresto, V., Ridgway, S., & Mariotti, J.-M. 1997, A&A, 121, 379
Coudé du Foresto, V., Bordé, P. J., Mérand, A., et al. 2003, in Interferometry for Optical Astronomy II, ed. W. A. Traub, Proc. SPIE, 4838, 280
Cox, A. N. 1980, ARA&A, 18, 15
Evans, N. R., Sasselov, D., & Short, C. I. 2002, AJ, 567, 1121
Hestroffer, D. 1997, A&A, 327, 199
Ireland, M. J., Tuthill, P. G., Davis, J., & Tango, W. 2005, MNRAS, 361, 337
Kervella, P., Nardetto, N., Bersier, D., Mourard, D., & Coudé du Foresto, V. 2004a, A&A, 416, 941
Kervella, P., Ségransan, D., & Coudé du Foresto, V. 2004b, A&A, 425, 1161
Kervella, P., Mérand, A., Coudé du Foresto, V., & Perrin, G. 2006, A&A, 448, 623
Mérand, A., Bordé, P., & Coudé du Foresto, V. 2005a, A&A, 433, 1555
Mérand, A., Kervella, P., Coudé Du Foresto, V., et al. 2005b, A&A, 438, L9
Michelson, A. A., & Pease, F. G. 1921, ApJ, 53, 249
Moskalik, & Gorynya 2005, Acta Astronomica, 55, 247
Perrin, G. 2003, A&A, 596, 702
Perrin, G., Ridgway, S. T., Mennesson, B., et al. 2004, A&A, 426, 279
Suh, K.-W. 1999, MNRAS, 304, 389
Szabados, L. 2003, Commmunications of the Konkoly Observatory Hungary, 103, 115
ten Brummelaar, T. A., McAlister, H. A., Ridgway, S. T., et al. 2005, ApJ, 628, 453
Wielen, R., Jahreiss, H., Dettbarn, C., Lenhardt, H., & Schawn, H. 2000, A&A, 360, 399